

Accepted Manuscript

Zinc phthalocyanine coupled with UIO-66 (NH₂) via a facile condensation process for enhanced visible-light-driven photocatalysis

Qian Liang, Miao Zhang, Zihui Zhang, Changhai Liu, Song Xu, Zhongyu Li



PII: S0925-8388(16)32465-3

DOI: [10.1016/j.jallcom.2016.08.087](https://doi.org/10.1016/j.jallcom.2016.08.087)

Reference: JALCOM 38589

To appear in: *Journal of Alloys and Compounds*

Received Date: 10 June 2016

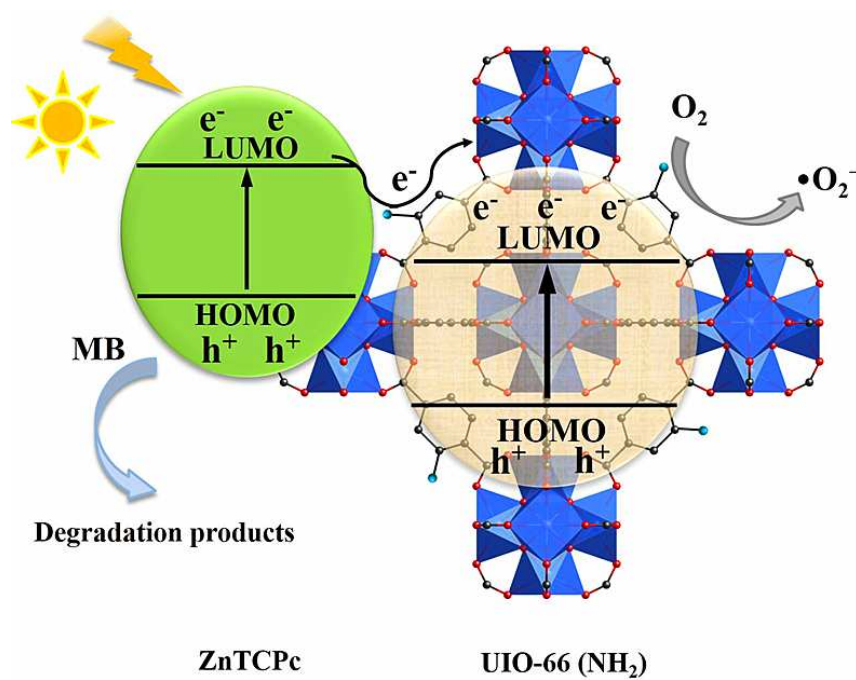
Revised Date: 23 July 2016

Accepted Date: 11 August 2016

Please cite this article as: Q. Liang, M. Zhang, Z. Zhang, C. Liu, S. Xu, Z. Li, Zinc phthalocyanine coupled with UIO-66 (NH₂) via a facile condensation process for enhanced visible-light-driven photocatalysis, *Journal of Alloys and Compounds* (2016), doi: 10.1016/j.jallcom.2016.08.087.

This is a PDF file of an unedited manuscript that has been accepted for publication. As a service to our customers we are providing this early version of the manuscript. The manuscript will undergo copyediting, typesetting, and review of the resulting proof before it is published in its final form. Please note that during the production process errors may be discovered which could affect the content, and all legal disclaimers that apply to the journal pertain.

Graphical abstract



ZnTCPC was immobilized on UIO-66 (NH₂) covalently and the photocatalytic degradation of methylene blue (MB) was investigated under visible irradiation.

Zinc phthalocyanine coupled with UIO-66 (NH₂) via a facile condensation process for enhanced visible-light-driven photocatalysis

Qian Liang^{a, *}, Miao Zhang^a, Zihui Zhang^a, Changhai Liu^b, Song Xu^a, Zhongyu Li^{a, *}

^aJiangsu Key Laboratory of Advanced Catalytic Materials and Technology, School of Petrochemical Engineering, Changzhou University, Changzhou 213164, PR China.

^bJiangsu Collaborative Innovation Center of Photovoltaic Science and Engineering, School of Materials Science & Engineering, Changzhou University, Changzhou 213164, PR China.

* Corresponding authors: Zhongyu Li, E-mail: zhongyuli@mail.tsinghua.edu.cn; Qian Liang, E-mail: qianliang@cczu.edu.cn, Tel.: +86 519 86334771; Fax: +86 519 86334771.

Abstract:

Metal-organic frameworks (MOFs) have shown a great potential for water treatment as an environmentally friendly photocatalyst. In this work, a zirconium based MOF, UIO-66 (NH₂) covalently coupled with zinc phthalocyanine (ZnTCPc) was prepared via a facile condensation process. Compared with the mixture of ZnTCPc and UIO-66 (Zr) by impregnation, ZnTCPc/UIO-66 (NH₂) presented an enhanced photocatalytic activity for the degradation of methylene blue (MB) under visible-light irradiation. The formation of strong covalent bonds and synergistic integration between ZnTCPc and UIO-66 (NH₂) was proved by characterization results such as transmission electron microscopy, X-ray photoelectron spectra and Fourier transform infrared spectroscopy. Additionally, ZnTCPc/UIO-66 (NH₂) photocatalyst retained excellent stability after five recycles, and the photocatalytic mechanism was investigated systematically. This work demonstrates a high potential of using porous MOFs-based materials not only as supports but as electron acceptors to trigger the reaction for coupling MOFs with dye, fabricating novel MOFs-dye nanocomposite systems and enhancing their photostability and photocatalytic activity.

Keywords: Metal-organic framework; Zinc phthalocyanine; Photocatalytic degradation

1. Introduction

With growing concerns regarding a clean environment and human health, technologies with high efficiency and low cost to reduce the pollutant contents of wastewater are urgently needed [1]. Various homogeneous and heterogeneous

photocatalysts systems have been widely studied and employed in the past few decades, including TiO₂, g-C₃N₄, graphene, metal-organic frameworks (MOFs), etc [2-6]. Among the reported photocatalytic materials, MOFs as a new class of porous crystalline networks synthesized by assembling metallic ions with organic ligands attracts more attentions in photocatalysis field [7-12]. Among these MOFs, zirconium based MOFs (UIO-66 (Zr) and UIO-66 analogies), associated with high surface area and superior chemical stability to water, not only possess the cage-like structure and high surface area to accommodate the nanoparticles and disperse the entrapped nanoparticles, but serve as the semiconductor material itself [13]. Sha et al. reported Ag₂CO₃/UIO-66 (Zr) could decompose rhodamine B (RhB) under visible-light irradiation [14]. Although UIO-66 series are potential candidates for the photocatalyst, compared with the inorganic photocatalysts and some commercial standards, pristine UIO-66 series failed to achieve satisfactory photocatalytic activities because of the limited light absorption [15, 16]. Therefore, it is necessary to develop a high-efficient visible-light driven photocatalyst to extend its spectral response to higher absorption wavelength.

A few attempts have been made to enhance the visible light response of UIO-66 (Zr) and UIO-66 analogies, such as combination with other components, like noble metals, semiconductors and carbon materials [17-19]. Zinc phthalocyanine (ZnPc) and its derivatives as typical organic semiconductors possess wide visible light response, which can be employed to sensitize other semiconductor materials for enhancement of photocatalytic activity [20-23]. However, the traditional ZnPc suffers

from the aggregation ascribed to its intrinsic large π -conjugation [24], and therefore, MOFs with the high surface area and desirable porosity can confine the aggregation of ZnPc and maximize the active sites. Based on the properties of UIO-66 and ZnPc, it is worthy to present an efficient approach to combine UIO-66 with ZnPc for the visible-light-driven photocatalysis. To our knowledge, the photocatalytic properties of UIO-66 incorporated with dyes have remained unexplored.

Herein we prepared composites combining zinc tetracarboxy phthalocyanine (ZnTCPc) with UIO-66 (Zr) and UIO-66 (NH₂), respectively. ZnTCPc/UIO-66 (Zr) were obtained by a simple impregnation method, while ZnTCPc was immobilized on UIO-66 (NH₂) covalently via *N*-(3-dimethylaminopropyl)-*N'*-ethylcarbodiimide hydrochloride (EDC)/*N*-hydroxysuccinimide (NHS) activation and amide formation. The photocatalytic performances were evaluated by the degradation of methylene blue (MB) under visible-light irradiation, and the results show that ZnTCPc/UIO-66 (Zr) and ZnTCPc/UIO-66 (NH₂) with different interactions have distinct effects on the photocatalytic activity. Compared with ZnTCPc/UIO-66 (Zr), ZnTCPc/UIO-66 (NH₂) with stronger covalent bonds and synergistic integration exhibited higher photocatalytic activity. Moreover, the ZnTCPc/UIO-66 (NH₂) composite also presents acceptable stability during the degradation experiments. In addition, some typical scavengers were added to identify the active species, and the possible photocatalytic mechanism was investigated systematically.

2. Experimental

2.1 Synthesis of UIO-66 (Zr) and UIO-66 (NH₂)

In a typical synthesis, ZrCl₄ (0.2332 g, 1.0 mmol) and terephthalic acid (0.1661 g, 1.0 mmol) or 2-NH₂-terephthalic acid (0.1812 g, 1.0 mmol) were dissolved in DMF (50 mL), and then the solution was transferred to a 100 mL Teflon-lined stainless steel autoclave [25, 26]. The autoclave was sealed and heated in an oven at 120 °C for 40 h under autogenous pressure. After being cooled naturally, the obtained sample was purified with anhydrous ethanol several times to make sure that the DMF molecules were eliminated, and then the off-white UIO-66 (Zr) or yellow UIO-66 (NH₂) product was dried at 80 °C for 24 h.

2.2. Synthesis of ZnTCPC

ZnSO₄·7H₂O (0.048 mol), trimellitic anhydride (0.176 mol), ammonium chloride (0.085 mol) and urea (1 mol) were mixed with ammonium molybdate tetrahydrate (0.004 mol). The mixture was dissolved in 10 mL nitrobenzene and then refluxed at 185 °C during 4 h. The dark blue solid obtained was purified with 0.1 M NaOH and 1 M HCl solution, respectively.

2.3. Synthesis of ZnTCPC/UIO-66 (Zr)

ZnTCPC sensitized UIO-66 (Zr) was prepared by an impregnation method. Typically, UIO-66 (Zr) (100 mg) was first dispersed in deionized water by ultrasonic treatment for 30 min to give an off-white solution. ZnTCPC (10 mg) dissolved in DMF (5 mL) was added into UIO-66 (Zr) solution drop by drop, and the mixture was stirred for 6 h. The obtained sample was purified with deionized water and ethanol

several times, and dried at 80 °C for 12 h. The nominal weight ratio of ZnTCPC to UIO-66 (Zr) was 10 wt %, and the actual content of zinc was shown in Table S1.

2.4. Synthesis of ZnTCPC/UIO-66 (NH₂)

Fig. 1 shows the preparation process of ZnTCPC/UIO-66 (NH₂). UIO-66 (NH₂) (100 mg) was dispersed in deionized water, and was subjected to sonication (100 W, 40 kHz) at 25 °C for 3 h. ZnTCPC (10 mg) was dissolved in DMF (5 mL) by ultrasonic treatment for 3 h to give a green solution. EDC (0.1 M) and NHS (0.1 M) were dissolved in deionized water, and then added into ZnTCPC solution [27, 28]. The ZnTCPC solution was added dropwise to the ultrasonic UIO-66 (NH₂) dispersion. After reacting for 6 h, the mixture was filtered and washed with deionized water and ethanol several times. The obtained ZnTCPC/UIO-66 (NH₂) was dried at 80 °C for 12 h. The nominal weight ratio of ZnTCPC to UIO-66 (NH₂) was 10 wt %, and the content of zinc was shown in Table S1.

2.5 Characterization

Powder X-ray diffraction (PXRD) patterns were recorded with a Shimadzu XRD 6000 X-ray diffractometer using Cu K α ($\lambda = 0.15406$ nm) radiation with a nickel filter operating at 40 kV and 10 mA. The patterns were compared with JCPDS reference data for phase identification. The surface morphology of the catalyst was observed by field emission scanning electron microscopy (FESEM) on a Quanta 200F instrument using accelerating voltages of 5 kV. Samples for SEM were dusted on an adhesive conductive carbon belt attached to a copper disk, coated with 10 nm Au prior to

measurement. The TEM images were carried out using a JEOL JEM 2100 electron microscope equipped with a field emission source at an accelerating voltage of 200 kV. Fourier transform infrared spectroscopy (FT-IR) spectra were obtained on an FTS-3000 spectrophotometer manufactured by American Digilab Company. The measured wafer was prepared as KBr pellet with the weight ratio of sample to KBr, 1/100. Raman spectra were measured at room temperature using a LabRAM XploRA Raman spectrometer (Horiba Jobin Yvon France) with a 532 nm laser focused on a spot about 3 nm diameter. Specific surface area was measured by adsorption-desorption of N₂ gas at 77 K with a Micromeritics ASAP 2000 gas sorption analyzer. Before the measurements, the samples were outgassed at 160 °C for 10 h. X-ray photoelectron spectra (XPS) were recorded on a Perkin-Elmer PHI-1600 ESCA spectrometer using Mg K α (h ν = 1253.6 eV) X-ray source. TGA data were obtained using a Perker Elmer TGA6 instrument under N₂ flow. Electron paramagnetic resonance (EPR) measurements were carried out on a Bruker model A300 spectrometer. UV-Vis diffused reflectance spectra (DRS) experiments were performed on a UV-Vis spectrophotometer (Hitachi U-4100) with the integration sphere diffuse reflectance attachment. ¹H NMR spectrum was recorded on a Bruker AV-300 spectrometer.

2.6 Evaluation of the photocatalytic activity

The photocatalytic activity was evaluated by the degradation of MB under visible light irradiation. A 500 W Xe arc lamp with an UV cut-off filter ($\lambda \geq 420$ nm) was used as a visible light source. A suspension containing a powdered catalyst (20 mg)

and a fresh aqueous solution of MB (100 mL, 15 mg/L) were magnetically stirred in the dark for about 20 min to establish an adsorption-desorption equilibrium of MB species. To measure the dye degradation, a 1.5 mL sample of the reaction suspension was collected after irradiation for a certain period, and the photocatalyst was removed by centrifugation (5000 rpm for 20 min) before the absorption spectroscopy measurements. The filtrate was analyzed by a 759 UV-vis spectrophotometer (Shanghai Precision & Scientific Instrument Co., Ltd.). To evaluate the photostability of the photocatalysts, samples were separated from the suspension after photocatalytic degradation reaction for 120 min, and then collected by centrifugation and dried at 50 °C overnight. The recovered photocatalysts were reused for subsequent cycles of photocatalytic degradation under the same conditions. The photocatalytic mechanism was investigated by different scavengers to compete with the potential active species that may be involved in the degradation process of MB. Benzoquinone (BQ), ethylenediaminetetraacetic acid disodium salt (EDTA-2Na) and isopropyl alcohol (IPA) were introduced as scavengers for superoxide radical anions ($\bullet\text{O}_2^-$), holes (h^+) and hydroxyl radicals ($\bullet\text{OH}$), respectively.

3. Results and discussion

3.1. Material characterization

Fig. S1 shows the XRD patterns of the pure ZnTCPC, UIO-66 (Zr), UIO-66 (NH_2) and their composites. For UIO-66 (Zr) and UIO-66 (NH_2) samples, all the diffraction peaks can be well matched with the previous reports [29, 30], exhibiting the excellent crystallinity. After the deposition of ZnTCPC, the characteristic diffraction of ZnTCPC

at 26.3° are not detected from XRD pattern for ZnTCPc/UIO-66 (Zr) or ZnTCPc/UIO-66 (NH₂). And there is no obvious loss of crystallinity in the XRD patterns of the above composites, indicating that the integrity of the UIO-66 (Zr) and UIO-66 (NH₂) frameworks is both maintained well during the different preparation processes. These above results are possible due to the following reasons: (i) the content of ZnTCPc is relatively low, and the ZnTCPc nanoparticles have small particle size and well dispersion in the ZnTCPc/UIO-66 (Zr); (ii) as for the ZnTCPc/UIO-66 (NH₂), the covalent structure has no obvious effect on the crystal structure of UIO-66 (NH₂) [31].

Fourier transform infrared (FT-IR) and Raman spectroscopies were applied to further characterize the hybrids, as shown in the Fig. 2 and Fig. S2. In the FT-IR spectra of UIO-66 (Zr) and UIO-66 (NH₂), the absorption peaks between 600-800 cm^{-1} correspond to Zr-O₂ as longitudinal and transverse modes, while intense doublet at 1433 and 1389 cm^{-1} (labelled with blue dot) of UIO-66 (NH₂) can be assigned to the stretching modes of the carboxylic groups in the BDC-NH₂ ligands [32]. In the spectrum of ZnTCPc, O-H stretching at 3136 cm^{-1} , C=O stretching at 1591 cm^{-1} , and O-H bending at 1339 cm^{-1} prove the existence of -COOH. As for the ZnTCPc/UIO-66 (Zr) composite prepared by the simple impregnation, all of the IR vibration bands are fully consistent with those of the pristine UIO-66 (Zr), suggesting the composites have the same chemical structure as the pristine UIO-66 (Zr). Most importantly, after the ZnTCPc was reacted with UIO-66 (NH₂) covalently, the absorption peaks were attributed to amino groups in the BDC-NH₂ ligands between 1030 and 1130 cm^{-1}

disappear. Besides, the typical signal of CO-NH₂ at 1620 cm⁻¹ and the characteristic absorption of the N-H stretching band at 3344 cm⁻¹ appears in the spectra of the ZnTCPc/UIO-66 (NH₂), further confirming that the -COOH reacted with -NH₂ with EDA successfully [33, 34]. Fig. S2 shows the Raman spectra at room temperature of the as-prepared samples. The vibrational peaks of UiO-66 (Zr) are present between 650 and 1700 cm⁻¹, attributed to BDC organic linkers. The vibrations at 650-900 cm⁻¹, 1140 cm⁻¹, 1430-1625 cm⁻¹ are assigned to C-H out of plane bending, C-H in plane bending and C-C stretching, respectively [35]. While the Raman spectrum of UIO-66 (NH₂) is not available because this material is fluorescent and the detection of its typical spectroscopic features is not possible [36, 37]. As for ZnTCPc/UIO-66 (Zr), the vibrational peaks of UIO-66 (Zr) disappear after the integration of ZnTCPc, indicating that the appearance of ZnTCPc may cause some influence on the optical property of UIO-66 (Zr).

Surface areas and pore structure of the as-prepared samples were investigated using N₂ adsorption-desorption measurements (Fig. 3). The nitrogen adsorption isotherms of all the as-prepared samples indicate a steep nitrogen gas uptake at low relative pressure, and belong to the typical type I, revealing microporous structure. The BET surface areas of pure UIO-66 (Zr) and UIO-66 (NH₂) are 958 and 842 m² g⁻¹, respectively. The Horvath-Kawazoe (HK) micropore size distribution of UIO-66 (NH₂) shows two major pores at 0.9 and 0.7 nm. After introduction of ZnTCPc, the BET surface areas of the composite materials (ZnTCPc/UIO-66 (Zr) and ZnTCPc/UIO-66 (NH₂)) decrease to 630 and 575 m² g⁻¹, respectively, due to pore blockage by the

ZnTCPc nanoparticles and ZnTCPc complex, respectively. It should be noted that although the BET surface areas of the composites are smaller than that of pure UIO-66 (Zr) or UIO-66 (NH₂), they are still much higher than most of other ZnPc and ZnPc-based materials. A high specific surface area of photocatalysts can supply more surface active sites and make charge carrier transport easier, leading to an enhancement of the photocatalytic performance [38].

The TEM and SEM images of ZnTCPc, UIO-66 (Zr), UIO-66 (NH₂), ZnTCPc/UIO-66 (Zr) and ZnTCPc/UIO-66 (NH₂) samples are shown in Fig. 4 and Fig. S3. It can be seen from the TEM image of ZnTCPc/UIO-66 (Zr) composite that ZnTCPc nanoparticles are dispersed on the external surface of UIO-66 (Zr) compared with the bare ZnTCPc since the UIO-66 (Zr) with high surface area can prevent the aggregation of ZnTCPc during the preparation process. Interestingly, there are no obvious nanoparticles in the ZnTCPc/UIO-66 (NH₂) composite, different from the composite simply mixed ZnTCPc and UIO-66 (Zr), indicating that not only the introduction of ZnTCPc has no effect on the morphology of UIO-66(NH₂) but also the interaction between ZnTCPc and UIO-66 (NH₂) could be formed by chemical bond.

The thermal stability of the samples was evaluated by thermal gravimetric analysis (TGA, Fig. 5). UIO-66 (Zr) shows a gradual mass loss up to ~200 °C, corresponding to the removal of adsorbed guest molecules from the porous surface. A plateau is shown in the temperature range of 300-450 °C, indicating high thermal stability of the sample, which is followed by the complete decomposition of the framework at around 500 °C. Compared to UIO-66 (Zr), the thermal stability of UIO-66 (NH₂) slightly

decreases, which is stable up to 330 °C and has a 43% weight loss (320-480 °C) corresponding to the decomposition of the BDC-NH₂ linkers [32, 39]. For the pure ZnTCPc, TGA analysis shows weight loss of ZnTCPc at three different temperature ranges and its total weight loss is up to 80%. The composites ZnTCPc/UIO-66 (Zr) and ZnTCPc/UIO-66 (NH₂) have the similar curves but higher stability properties compared with the pristine structure (UIO-66 (Zr) and UIO-66 (NH₂)), which is ascribed to the formation of strong interaction between ZnTCPc and UIO-66.

Electron paramagnetic resonance (EPR) analysis was carried out to investigate the electronic band structure of the samples. The EPR spectra of powdered UIO-66 (NH₂), ZnTCPc and ZnTCPc/UIO-66 (NH₂) were measured at room temperature in Fig. S4. The pure UIO-66 (NH₂) shows three EPR lines at 2.036, 2.026 and 2.015, while the EPR lines of ZnTCPc are calculated as 2.019 and 2.015. The line at 2.015 is due to the defects in the Zr₆O₃₂ core and the two EPR lines at 2.036 and 2.026 are from •O₂⁻ species adsorbed on Zr³⁺ sites [40]. It is obvious that the intensity of the EPR lines increases with integration of ZnTCPc in UIO-66 (NH₂), which may be caused by the •O₂⁻ species formed from the photogenerated electrons [41]. The active •O₂⁻ species could be stabilized in the porosity structure of UIO-66 (NH₂) because of its strong conjugated interaction with ZnTCPc compound, which is consistent with the analysis of photocatalytic mechanism. As expected, this introduction of ZnTCPc that can induce synergetic effect sufficiently enhances the photoactivity of UIO-66 (NH₂) and ZnTCPc.

As the photoabsorption property plays a key role in determining the photocatalytic activity, the UV-vis diffuse reflectance spectra (DRS) of the samples have been measured, as shown in Fig. 6. UiO-66 (Zr) spectrum characterized by an absorption edge around 310 nm is ascribed to π - π^* electronic transitions of the aromatic ring. Although frontier orbitals of UiO-66 (NH_2) show a localized electronic state, strong photo-absorption bands from 260 nm to 430 nm in UiO-66(NH_2) are observed attributed to charge transfer process from sets of the ligand to Zr- O_2 cluster. Compared with UiO-66 (Zr), the absorption edge of UiO-66 (NH_2) was red shifted, which could be attributed to the addition of amino group with lone pair electrons, leading to the lift of the highest occupied molecular orbital (HOMO) level [30]. As for ZnTCPc/UiO-66 (Zr) composite, new absorption peaks at 400 nm and 600-750 nm belonging to ZnTCPc absorption band are observed, and the absorption edge of UiO-66 (Zr) in the composite is slightly red shifted. The absorption peak of the ZnTCPc/UiO-66 (NH_2) around 600-750 nm also originates from the absorption of ZnTCPc, but absorption peak at about 400 nm attributed to ZnTCPc is not obvious. Besides, ZnTCPc/UiO-66 (NH_2) shows much broader absorption band through the entire visible light region, and exhibits intense and excellent visible light absorption properties. It can be concluded that the formation of a chemical interaction between ZnTCPc (-COOH groups) and UiO-66 (NH_2) via a condensation reaction may induce a synergetic effect to enhance the photoactivity of UiO-66 (NH_2). In addition, as shown in Fig. 7, the UV-vis spectra of ZnTCPc in DMF solution show a good absorption on the wavelength of light about 680 nm. The absorption of

ZnTCPc/UIO-66 (Zr) appears around 680 nm which is ascribed to the absorption of ZnTCPc. Compared to the ZnTCPc/UIO-66 (Zr) prepared by impregnation, the absorption of ZnTCPc/UIO-66 (NH₂) reacted with EDC demonstrates about ~8 nm red-shift, which should arise from the covalent amide structure [31].

The chemical states C, N and Zr of the as-prepared photocatalysts are probed with XPS, as shown in Fig. 8 and Fig. S5. Fig. 8a shows the normalized C1s high resolution XPS spectra of UIO-66-NH₂, ZnTCPc and their composite. For pure UIO-66-NH₂ nanocrystals, there are three peaks at 284.5 eV, 286.2 eV and 288.5 eV, which belong to the sp² C, C-N and O-C-O groups, respectively [42]. The pure ZnTCPc show two peaks at 284.5 eV and 288 eV, arising from sp² C and C=O/C=N groups [31]. The composite of UIO-66-NH₂ and ZnTCPc has two sets of C1s XPS peaks, which not only contain those characteristic peaks of UIO-66-NH₂ and ZnTCPc, but also contain a new peak at 287.5 eV. It demonstrates that there is amide (-CO-NH), generating from condensation reaction between amino and carboxyl functional group. This can be further confirmed from normalized N1s XPS spectra in Fig. 8b. The two N1s peak at 400 eV and 401.8 eV are corresponding to -NH₂ and -NH groups, while the ratio of -NH and -NH₂ in composite increases compared with that of pure UIO-66-NH₂ nanocrystals, suggesting that the successful reaction between UIO-66-NH₂ and ZnTCPc. Interestingly, there is a new doublet at 183.3 eV and 185.7 eV for Zr3d XPS spectra compared with UIO-66-NH₂, as shown in Fig. S5 and Table S2. The significant shift ($\Delta = +1.0$ eV) of the Zr 3d binding energies towards a higher energy demonstrates that strong electron-withdrawing effect of ZnTCPc for the metal

component [37]. So it can be concluded that the electronic structure of composite is altered through the condensation reaction and the electron-withdrawing effect of ZnTCPc toward metal component.

3.2. Photocatalytic activity and stability

As shown in Fig. 9, the photocatalytic activity of the as-prepared samples was evaluated by the degradation of MB in aqueous solution under visible light irradiation ($\lambda \geq 420$ nm). When ZnTCPc was added alone, there was no obvious change in the concentration of MB in the presence of ZnTCPc, suggesting that ZnTCPc had no obvious photocatalytic activity for the degradation of MB. In the presence of pristine UIO-66 (Zr) and UIO-66 (NH₂), MB concentration was gradually decreased and the removal rate are 58% and 56% within 120 min, respectively. It should be noted that although the photocatalytic activity of pristine UIO-66 (Zr) is similar to that of UIO-66 (NH₂), ZnTCPc/UIO-66 (Zr) composite showed a relatively better photocatalytic performance with a removal rate of 68%, which could be ascribed to synergetic effect between ZnTCPc and UIO-66 (Zr) [43]. ZnTCPc/UIO-66 (NH₂) with stable covalent bonds exhibited the highest catalytic activity due to the co-modifications of ZnTCPc and UIO-66 (NH₂). The catalytic activities are in the order of ZnTCPc < UIO-66 (NH₂) < UIO-66 (Zr) < ZnTCPc/UIO-66 (Zr) < ZnTCPc/UIO-66 (NH₂). In Fig. S6, the reaction rate constant (k) described as a pseudo-first-order reaction mode, can be calculated from the slope of the linear fit of $\ln(C_t/C_0)$ vs t . The ZnTCPc/UIO-66 (NH₂) shows a k value of 0.0168 min⁻¹ which is 1.84, 2.37 and 9.33 times higher than that of ZnTCPc/UIO-66 (Zr) (0.0091 min⁻¹),

bare UIO-66 (NH₂) (0.0071 min⁻¹) and ZnTCPC (0.0018 min⁻¹), respectively. The stability of photocatalysts is a major concern for their practical utility in real applications. We therefore investigated the stability of ZnTCPC/UIO-66 (NH₂) composite in photocatalytic degradation of MB, as shown in Fig. 10. Although there is a decrease in the degradation rate for each cycle, more than 70% of MB can still be degraded in the fourth cycle, indicating its high stability in the photocatalytic reaction under visible-light irradiation.

3.3. Photocatalytic mechanism

The photocatalytic mechanism of the ZnTCPC/UIO-66 (NH₂) composite was investigated through determining the potential roles of h⁺, •O₂⁻ and •OH during the degradation, since they are known as the three main active species involved in the photocatalytic process. To identify the contributions of these active species, three different scavengers (EDTA, BQ and IPA) were separately added into the degradation system of MB to attempt to trap h⁺, •O₂⁻ and •OH. As shown in Fig. 11, the addition of IPA does not cause any change in the MB degradation rate, which suggests that •OH should not be an important contributor to the photocatalytic process. However, the degradation rate obviously decreases at the presence of EDTA significantly, indicating that photogenerated holes should be one of the main active species participating in the decomposition process of MB. While the addition of BQ partially suppresses the degradation rate, and shows a significant effect on the *k* value which decreases obviously from 0.01721 min⁻¹ to 0.01002 min⁻¹, showing that •O₂⁻ is also a dominant reactive species.

To further understand the underlying mechanism for electrical conduction properties, the flat band position determined from the previous literature is approximately -0.6 V, -0.8 V and -1.5 V for UIO-66 (Zr), UIO-66 (NH₂) and ZnTCPc, respectively [13, 30, 31, 44]. These data, together with the band gap energy estimated from UV-visible spectra, allow us to present the absolute energy scheme, including HOMO and LUMO positions. A schematic diagram is shown in Fig. S7, which describes the band positions and band gaps of UIO-66 (Zr), UIO-66 (NH₂) and ZnTCPc samples. The photogenerated electron-hole pairs of UIO-66 (Zr), UIO-66 (NH₂) and ZnTCPc simultaneously arises from visible light irradiation. Since the LUMO of ZnTCPc is higher than that of UIO-66 (Zr)/UIO-66 (NH₂), the excited electrons of ZnTCPc could be easily injected into UIO-66 (Zr)/UIO-66 (NH₂), making electron-hole separation more efficient and reducing the probability of recombination.

Based on the above results and discussions, we propose the following mechanism illustrated in Fig. 12: the dye molecules adsorbed on porous UIO-66 (Zr)/UIO-66 (NH₂) are excited under visible light irradiation, and then the photogenerated electrons are injected into UIO-66 (Zr)/UIO-66 (NH₂). Meanwhile, the active species holes produced from MOFs are injected into the HOMO of ZnTCPc and the photo-generated holes are collected in the HOMO of ZnTCPc. Nevertheless, ZnTCPc/UIO-66 (NH₂) exhibited much higher photocatalytic activity than that of ZnTCPc/UIO-66 (Zr) in our work. The main reasons can be described as follows: the Zr-oxo clusters within UIO-66 (NH₂) can behave as quantum dots surrounded by terephthalate ligands with the NH₂ groups (BDC-NH₂), which can act as antennae

absorbing light and be able to efficiently transfer the electrons to the inorganic zirconium-oxygen clusters part [44]. Moreover, the excited electrons could be transferred more effectively supported by the amide covalent bonds in the ZnTCPC/UIO-66 (NH₂) composite. Due to the localized electronic state in UIO-66 (NH₂), the excited electrons located in the LUMO cannot diffuse into other positions [17]. However, the electrons can be transferred to O₂ molecules diffusing into pores and adsorbing on the Zr³⁺ sites, beneficial for the formation of superoxide radical •O²⁻ and Zr⁴⁺ ion. Therefore, the chemical bonds and synergistic effect between UIO-66 (NH₂) and ZnTCPC should be the intrinsic factor for its better photosensitization than ZnTCPC/UIO-66 (Zr).

4. Conclusion

Zr-based MOF combined with ZnTCPC toward visible-light-driven photocatalytic degradation of MB has been successfully developed. The composite combining ZnTCPC and UIO-66 (NH₂) via a condensation reaction shows the highest photocatalytic activity in our work. The enhanced photocatalytic performance arises from the efficient separation of photogenerated electron-hole pairs and charge transfer in composite, because of the tight contact between ZnTCPCs and UIO-66(NH₂) via a covalent amide structure, rather than the simple physical interaction from an impregnation method. Besides, the ZnTCPC/UIO-66 (NH₂) composite is able to preserve most of its initial photocatalytic activity after four cycles of degradation experiments. The study on the photocatalytic mechanism of the ZnTCPC/UIO-66 (NH₂) composite implies that h⁺ and •O₂⁻ should be the major contributors to the

degradation process of MB. It is hoped that our work could provide a novel method for the design and fabrication of porous MOFs-dyes composites, which may offer more opportunities for photocatalytic applications.

Acknowledgements

This work was supported by the Natural Science Foundation of Jiangsu Province (Nos. BK20150259, BK20160277).

References

- [1] C.C. Chen, W.H. Ma, J.C. Zhao, *Semiconductor-mediated photodegradation of pollutants under visible-light irradiation*, *Chem. Soc. Rev.* 39 (2010) 4206-4219.
- [2] J.H. Park, S. Kim, A.J. Bard, *Novel carbon-doped TiO₂ nanotube arrays with high aspect ratios for efficient solar water splitting*, *Nano Lett.* 6 (2006) 24-28.
- [3] J.L. Li, X.T. Xu, X.J. Liu, C.Y. Yu, D. Yan, Z. Sun, L.K. Pan, *Sn doped TiO₂ nanotube with oxygen vacancy for highly efficient visible light photocatalysis*, *J. Alloys. Comp.* 679 (2016) 454-462.
- [4] T.G. Xu, L.W. Zhang, H.Y. Cheng, Y.F. Zhu, *Significantly enhanced photocatalytic performance of ZnO via graphene hybridization and the mechanism study*, *Appl. Catal. B: Environ.* 101 (2011) 382-387.

- [5] W.L. Shi, F. Guo, J.B. Chen, G.B. Che, X. Lin, *Hydrothermal synthesis of InVO₄/Graphitic carbon nitride heterojunctions and excellent visible-light-driven photocatalytic performance for rhodamine B*, *J. Alloys. Comp.* 612 (2014) 143-148.
- [6] H. Wang, X.Z. Yuan, Y. Wu, G.M. Zeng, X.H. Chen, L.J. Leng, Z.B. Wu, L.B. Jiang, H. Li, *Facile synthesis of amino-functionalized titanium metal-organic frameworks and their superior visible-light photocatalytic activity for Cr(VI) reduction*, *J. Hazard. Mater.* 286 (2015) 187-194.
- [7] M.A. Nasalevich, R. Becker, E.V. Ramos-Fernandez, S. Castellanos, S.L. Veber, M.V. Fedin, F. Kapteijn, J.N. Reek, J.I. Vlugt, J. Gascon, *Co@NH₂-MIL-125(Ti): cobaloxime-derived metal-organic framework-based composite for light-driven H₂ production*, *Energy Environ. Sci.* 8 (2015) 364-375.
- [8] H. Yang, X.W. He, F. Wang, Y. Kang, J. Zhang, *Doping copper into ZIF-67 for enhancing gas uptake capacity and visible-light-driven photocatalytic degradation of organic dye*, *J. Mater. Chem. A* 22 (2012) 21849-21851.
- [9] Y. Du, R.Z. Chen, J.F. Yao, H.T. Wang, *Facile fabrication of porous ZnO by thermal treatment of zeolitic imidazolate framework-8 and its photocatalytic activity*, *J. Alloys. Comp.* 551 (2013) 125-130.
- [10] T. Wen, D.X. Zhang, J. Zhang, *Two-dimensional copper(I) coordination polymer materials as photocatalysts for the degradation of organic dyes*, *Inorg. Chem.* 52 (2013) 12-14.

- [11] R.W. Liang, F.F. Jing, L.J. Shen, N. Qin, L. Wu, MIL-53(Fe) as a highly efficient bifunctional photocatalyst for the simultaneous reduction of Cr(VI) and oxidation of dyes, *J. Hazard. Mater.* 287 (2015) 364-372.
- [12] D.K. Wang, M.T. Wang, Z.H. Li, Fe-based metal-organic frameworks for highly selective photocatalytic benzene hydroxylation to phenol, *ACS Catal.* 5 (2015) 6852-6857.
- [13] L.J. Shen, S.J. Liang, W.M. Wu, R.W. Liang, L. Wu, CdS-decorated UiO-66(NH₂) nanocomposites fabricated by a facile photodeposition process: an efficient and stable visible-light-driven photocatalyst for selective oxidation of alcohols, *J. Mater. Chem. A.* 1 (2013) 11473-11482.
- [14] Z. Sha, H.S. Chana, J.S. Wu, Ag₂CO₃/UiO-66(Zr) composite with enhanced visible-light promoted photocatalytic activity for dye degradation, *J. Hazard. Mater.* 299 (2015) 132-140.
- [15] R. Lin, L.J. Shen, Z.Y. Ren, W.M. Wu, Y.X. Tan, H.R. Fu, J. Zhang, L. Wu, Enhanced photocatalytic hydrogen production activity via dual modification of MOF and reduced graphene oxide on CdS, *Chem. Commun.* 50 (2014) 8533-8535.
- [16] Y.P. Yuan, L.S. Yin, S.W. Cao, G.S. Xua, C.H. Lia, C. Xue, Improving photocatalytic hydrogen production of metal-organic framework UiO-66 octahedrons by dye-sensitization, *Appl. Catal. B: Environ.* 168-169 (2015) 572-576.

- [17] Z.Z. Gu, L.Y. Chen, B.H. Duan, Q. Luo, J. Liu, C.Y. Duan, *Synthesis of Au@UiO-66(NH₂) structures by small molecule-assisted nucleation for plasmon-enhanced photocatalytic activity*, *Chem. Commun.* 52 (2015) 116-119.
- [18] J.J. Zhou, R. Wang, X.L. Liu, F.M. Peng, C.H. Li, F. Teng, Y.P. Yuan, *In situ growth of CdS nanoparticles on UiO-66 metal-organic framework octahedrons for enhanced photocatalytic hydrogen production under visible light irradiation*, *Appl. Surf. Sci.* 346 (2015) 278-283.
- [19] T.W. Goh, C.X. Xiao, R.V. Maligal-Ganesh, X.L. Li, W.Y. Huang, *Utilizing mixed-linker zirconium based metal-organic frameworks to enhance the visible light photocatalytic oxidation of alcohol*, *Chem. Eng. Sci.* 124 (2015) 45-51.
- [20] K. Takanebe, K. Kamata, X. C. Wang, M. Antonietti, J. Kubota and K. Domen, *Photocatalytic hydrogen evolution on dye-sensitized mesoporous carbon nitride photocatalyst with magnesium phthalocyanine*, *Phys. Chem. Chem. Phys.* 12 (2010) 13020-13025.
- [21] Z.C. Guo, C.L. Shao, M.Y. Zhang, J.B. Mu, Z.Y. Zhang, P. Zhang, B. Chen, Y.C. Liu, *Dandelion-like Fe₃O₄@CuTNPc hierarchical nanostructures as a magnetically separable visible-light photocatalyst*, *J. Mater. Chem.* 21 (2011) 12083-12088.
- [22] X.H. Zhang, L.J. Yu, C.S. Zhuang, T.Y. Peng, R.J. Li, X.G. Li, *Highly asymmetric phthalocyanine as a sensitizer of graphitic carbon nitride for extremely efficient photocatalytic H₂ production under near-infrared light*, *ACS Catal.* 4 (2014) 162-170.

- [23] Y. Wan, Q. Liang, Z.Y. Li, S. Xu, X.J. Hu, Q.L. Liu, D.Y. Lu, Significant improvement of styrene oxidation over zinc phthalocyanine supported on multi-walled carbon nanotubes, *J. Mol. Catal. A: Chem.* 402 (2015) 29-36.
- [24] L.J. Yu, X.H. Zhang, C.S. Zhuang, L.Lin, R.J. Li, T.Y. Peng, Syntheses of asymmetric zinc phthalocyanines as sensitizer of Pt-loaded graphitic carbon nitride for efficient visible/near-IR-light-driven H₂ production, *Phys. Chem. Chem. Phys.* 16 (2014) 4106-4114.
- [25] Z. Sha, J.L. Sun, H.S. Chan, S. Jaenike, J.S. Wu, Bismuth tungstate incorporated zirconium metal-organic framework composite with enhanced visible-light photocatalytic performance, *RSC Adv.* 4 (2014) 64977-64984.
- [26] M. Pintado-Sierra, A.M. Rasero-Almansa, A. Corma, M. Iglesias, F. Sánchez, Bifunctional iridium-(2-aminoterephthalate)-Zr-MOF chemoselective catalyst for the synthesis of secondary amines by one-pot three-step cascade reaction, *J. Catal.* 299 (2013) 137-145.
- [27] E.D. Canto, M. Natali, D. Movia, S. Giordani, Photo-controlled release of zinc metal ions by spiropyran receptors anchored to single-walled carbon nanotubes, *Phys. Chem. Chem. Phys.* 14 (2012) 6034-6043.
- [28] J.H. Dai, Z.Y. Bao, L. Sun, S.U. Hong, G.L. Baker, M.L. Bruening, High-capacity binding of proteins by poly(acrylic acid) brushes and their derivatives, *Langmuir* 22 (2006) 4274-4281.

[29] N.Z. Shang, C. Feng, S.T. Gao, C. Wang, Ag/Pd nanoparticles supported on amine functionalized metal-organic framework for catalytic hydrolysis of ammonia borane, *Int. J. Hydrogen Energy*. 38 (2013) 11964-11972.

[30] L.J. Shen, W.M. Wu, R.W. Liang, R. Lin, L. Wu, Highly dispersed palladium nanoparticles anchored on UiO-66(NH₂) metal-organic framework as a reusable and dual functional visible-light-driven photocatalyst, *Nanoscale* 5 (2013) 9374-9382.

[31] W.Y. Lu, T.F. Xu, Y. Wang, H.G. Hu, N. Li, X.M. Jiang, W.X. Chen, Synergistic photocatalytic properties and mechanism of g-C₃N₄ coupled with zinc phthalocyanine catalyst under visible light irradiation, *Appl. Catal. B: Environ.* 180 (2016) 20-28.

[32] L. Valenzano, B. Civalieri, S. Chavan, S. Bordiga, M.H. Nilsen, S. Jakobsen, K.P. Lillerud, C. Lamberti, Disclosing the complex structure of UiO-66 metal organic framework: a synergic combination of experiment and theory, *Chem. Mater.* 23 (2011) 1700-1718.

[33] M.R. Armstrong, K.Y. Arredondo, C.Y. Liu, J.E. Stevens, A. Mayhob, B. Shan, S. Senthilnathan, C.J. Balzer, B. Mu, UiO-66 MOF and poly(vinyl cinnamate) nanofiber composite membranes synthesized by a facile three-stage process, *Ind. Eng. Chem. Res.* 54 (2015) 12386-12392.

[34] N. Li, Y.G. Wang, W. Cao, Y.H. Zhang, T. Yan, B. Du, Q. Wei, An ultrasensitive electrochemical immunosensor for CEA using MWCNT-NH₂ supported PdPt nanocages as labels for signal amplification, *J. Mater. Chem. A* 3 (2015) 2006-2011.

- [35] M. Kandiah, M.H. Nilsen, S. Usseglio, S. Jakobsen, U. Olsbye, M. Tilset, C. Larabi, E.A. Quadrelli, F. Bonino, K.P. Lillerud, *Synthesis and stability of tagged UiO-66 Zr-MOFs*, *Chem. Mater.* 22 (2010) 6632-6640.
- [36] E. Callini, P.A. Szilagyi, M. Paskevicius, N.P. Stadie, J. Rehaut, C.E. Buckley, A. Borgschulte, A. Züttel, *Stabilization of volatile $Ti(BH_4)_3$ by nanoconfinement in a metal-organic framework*, *Chem. Sci.* 7 (2016) 666-672.
- [37] J. Xu, S. He, H.L. Zhang, J.C. Huang, H.X. Lin, X.X. Wang, J.L. Long, *Layered metal-organic framework/graphene nanoarchitectures for organic photosynthesis under visible light*, *J. Mater. Chem. A* 3 (2015) 24261-24271.
- [38] S.T. Gao, W.H. Liu, C. Feng, N.Z. Shang, C. Wang, *A Ag-Pd alloy supported on an amine functionalized UiO-66 as an efficient synergetic catalyst for the dehydrogenation of formic acid at room temperature*, *Catal. Sci. Technol.* 6 (2016) 869-874.
- [39] Y.T. Han, M. Liu, K.Y. Li, Y. Zuo, Y.X. Wei, S.T. Xu, G.L. Zhang, C.S. Song, Z.C. Zhang, X.W. Guo, *Facile synthesis of morphology and sizecontrolled zirconium metal-organic framework UiO-66: the role of hydrofluoric acid in crystallization*, *CrystEngComm* 17 (2015) 6434-6440.
- [40] T. Maity, D. Saha, S. Koner, *Aromatic N-arylations catalyzed by copper-anchored porous zinc-based metal-organic framework under heterogeneous conditions*, *ChemCatChem* 6 (2014) 2373-2383.

- [41] J.L. Long, S.B. Wang, Z.X. Ding, S.C. Wang, Y.G. Zhou, L. Huang, X.X. Wang, *Amine-functionalized zirconium metal–organic framework as efficient visible-light photocatalyst for aerobic organic transformations*, *Chem. Commun.* 48 (2012) 11656-11658.
- [42] J. Yang, Y. Dai, X.Y. Zhu, Z. Wang, Y.S. Li, Q.X. Zhuang, J.L. Shi, J.L. Gu, *Metal-organic frameworks with inherent recognition sites for selective phosphate sensing through their coordination-induced fluorescence enhancement effect*, *J. Mater. Chem. A* 3 (2015) 7445-7452.
- [43] Q. Liang, M. Zhang, C.H. Liu, S. Xu, Z.Y. Li, *Sulfur-doped graphitic carbon nitride decorated with zincphthalocyanines towards highly stable and efficient photocatalysis*, *Appl. Catal. A: Gen.* 519 (2016) 107-115.
- [44] J. He, J.Q. Wang, Y.J. Chen, J.P. Zhang, D.L. Duan, Y. Wang, Z.Y. Yan, *A dye-sensitized Pt@UiO-66(Zr) metal-organic framework for visible-light photocatalytic hydrogen production*, *Chem. Commun.* 50 (2014) 7063-7066.

Figure captions

Fig. 1. Synthesis process of ZnTCPc/UIO-66 (NH₂).

Fig. 2. FT-IR spectra of ZnTCPc (a), UIO-66 (Zr) (b), UIO-66 (NH₂) (c), ZnTCPc/UIO-66 (Zr) (d) and ZnTCPc/UIO-66 (NH₂) (e).

Fig. 3. N₂ adsorption desorption isotherms of UIO-66 (Zr) (a), UIO-66 (NH₂) (b), ZnTCPc/UIO-66 (Zr) (c) and ZnTCPc/UIO-66 (NH₂) (d).

Fig. 4. TEM images of UIO-66 (Zr) (a), UIO-66 (NH₂) (b), ZnTCPc/UIO-66 (Zr) (c) and ZnTCPc/UIO-66 (NH₂) (d).

Fig. 5. Thermogravimetric analysis for pure ZnTCPc, UIO-66 (Zr), UIO-66 (NH₂), ZnTCPc/UIO-66 (Zr) and ZnTCPc/UIO-66 (NH₂).

Fig. 6. UV-vis diffusion reflectance absorption spectra (DRS) of ZnTCPc, UIO-66 (Zr), UIO-66 (NH₂), ZnTCPc/UIO-66 (Zr) and ZnTCPc/UIO-66 (NH₂).

Fig. 7. UV-vis spectra of ZnTCPc, UIO-66 (Zr), UIO-66 (NH₂), ZnTCPc/UIO-66 (Zr) and ZnTCPc/UIO-66 (NH₂).

Fig. 8. High resolution XPS spectra of C 1s (a) and N 1s (b) obtained from ZnTCPc, ZnTCPc/UIO-66 (NH₂) and UIO-66 (NH₂).

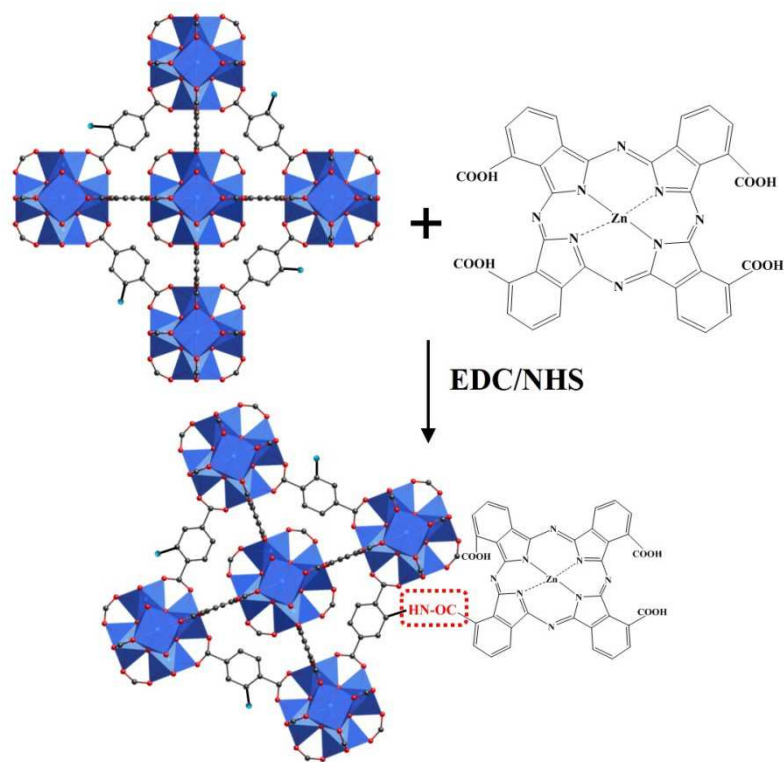
Fig. 9. Photocatalytic degradation of MB over the as-prepared samples under visible-light irradiation ($\lambda \geq 420$ nm).

Fig. 10. Photocatalytic recycle degradation of MB over ZnTCPc/UIO-66 (NH₂) under visible-light irradiation ($\lambda \geq 420$ nm).

Fig. 11. Effects of different scavengers on the degradation of MB in the presence of ZnTCPc/UIO-66 (NH₂) under visible-light irradiation.

Fig. 12. Schematic of photocatalytic degradation of MB over the ZnTCPc/UIO-66

(NH₂) under visible light irradiation.

**Fig. 1.** Synthesis process of ZnTCPc/UIO-66 (NH₂).

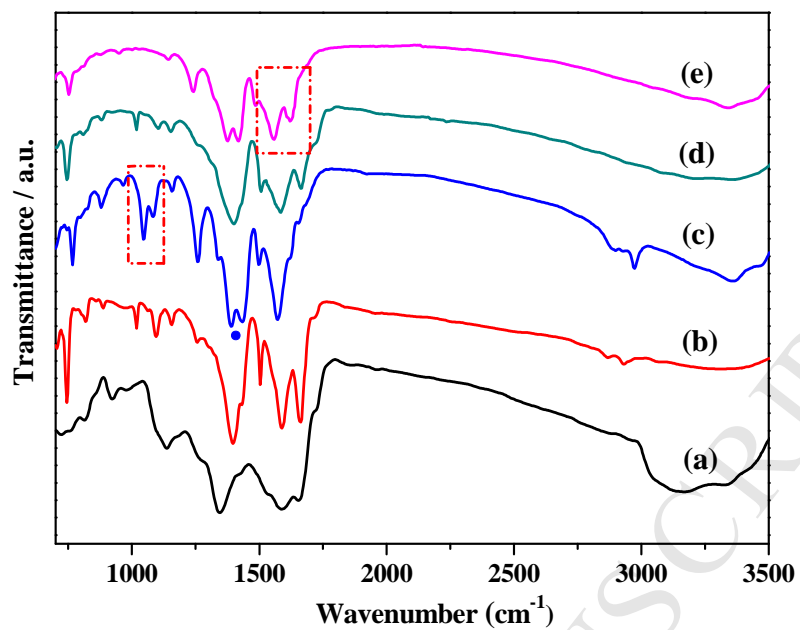


Fig. 2. FT-IR spectra of ZnTCPc (a), UIO-66 (Zr) (b), UIO-66 (NH₂) (c), ZnTCPc/UIO-66 (Zr) (d) and ZnTCPc/UIO-66 (NH₂) (e).

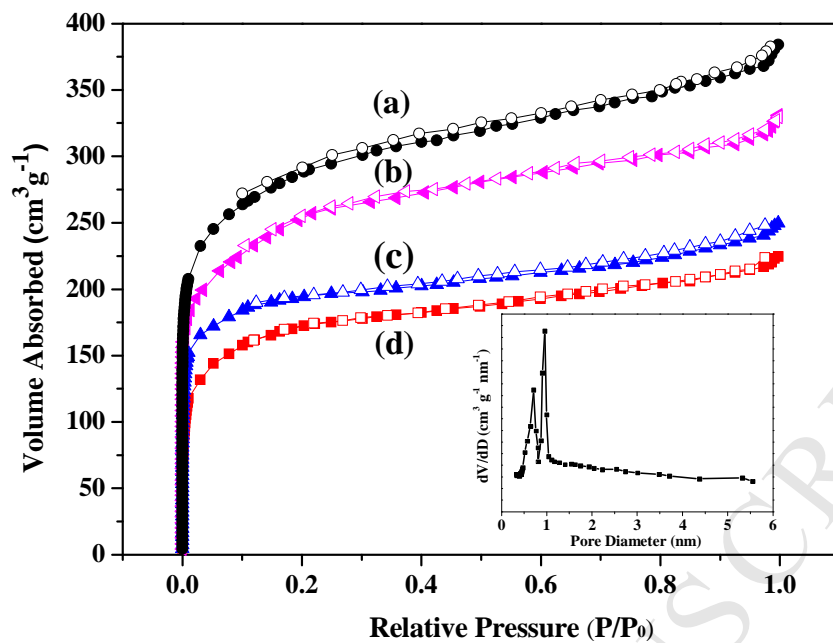


Fig. 3. N₂ adsorption desorption isotherms of UIO-66 (Zr) (a), UIO-66 (NH₂) (b), ZnTCPc/UIO-66 (Zr) (c), ZnTCPc/UIO-66 (NH₂) (d) and HK pore size distribution of UIO-66 (NH₂) (inset).

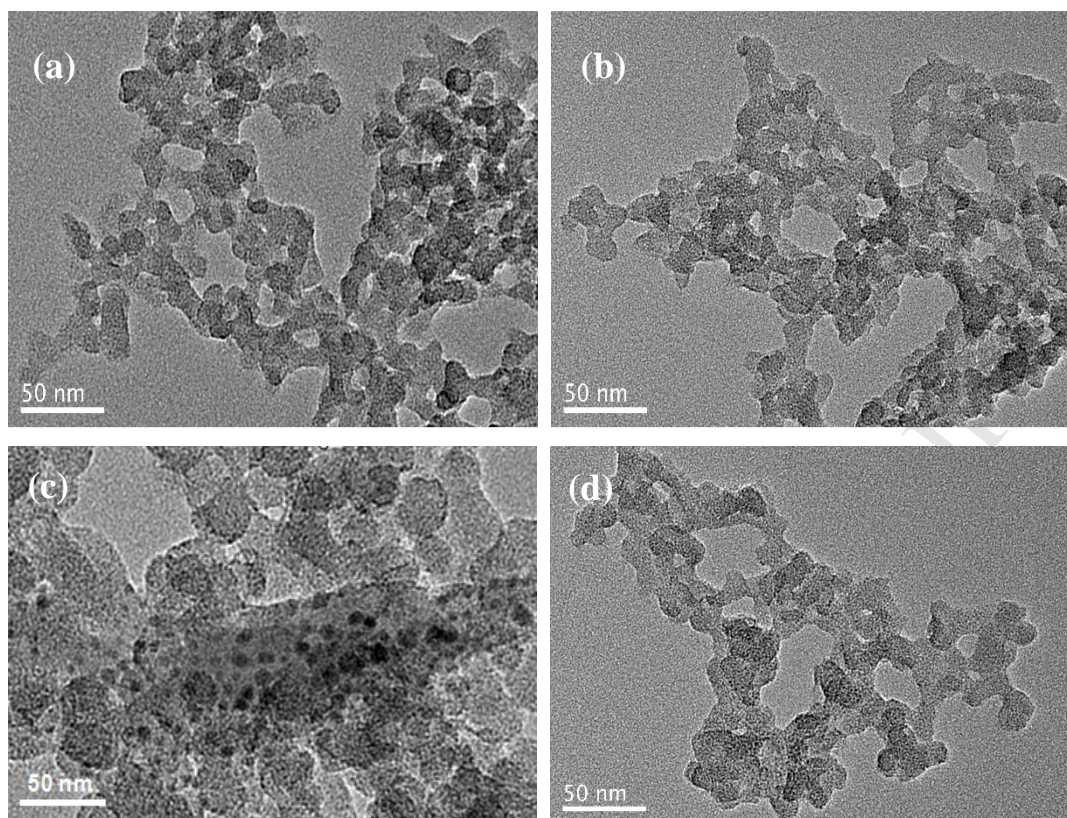


Fig. 4. TEM images of UIO-66 (Zr) (a), UIO-66 (NH₂) (b), ZnTCPc/UIO-66 (Zr) (c) and ZnTCPc/UIO-66 (NH₂) (d).

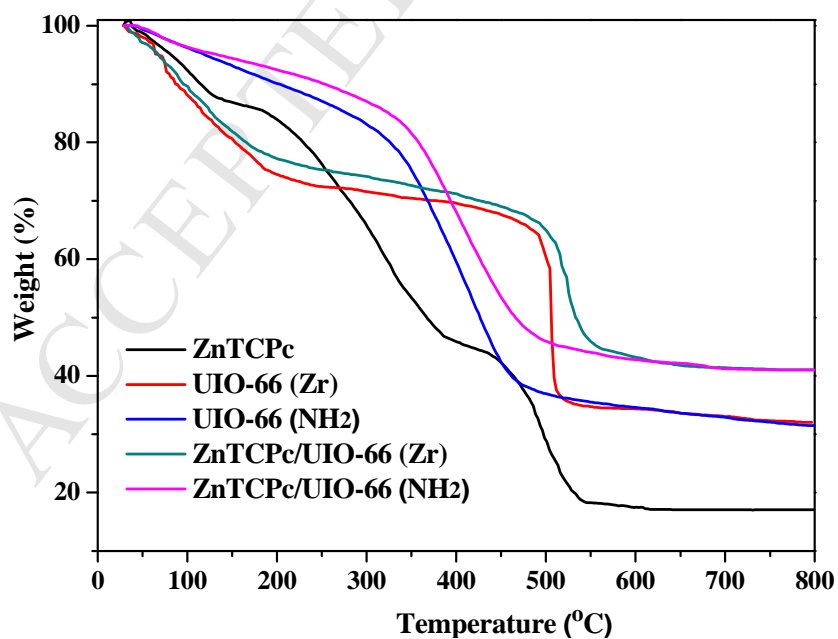


Fig. 5. Thermogravimetric analysis for pure ZnTCPc, UIO-66 (Zr), UIO-66 (NH₂), ZnTCPc/UIO-66 (Zr) and ZnTCPc/UIO-66 (NH₂).

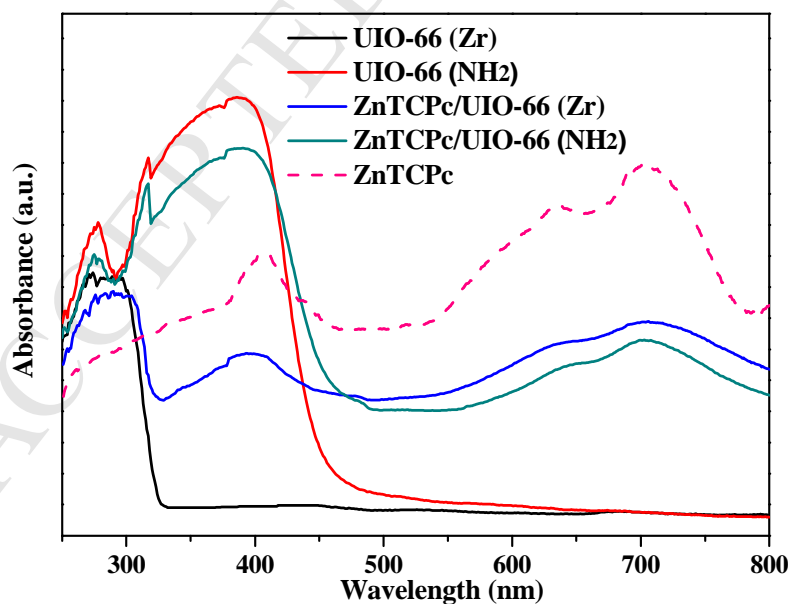


Fig. 6. UV-vis diffusion reflectance absorption spectra (DRS) of ZnTCPc, UIO-66 (Zr), UIO-66 (NH₂), ZnTCPc/UIO-66 (Zr) and ZnTCPc/UIO-66 (NH₂).

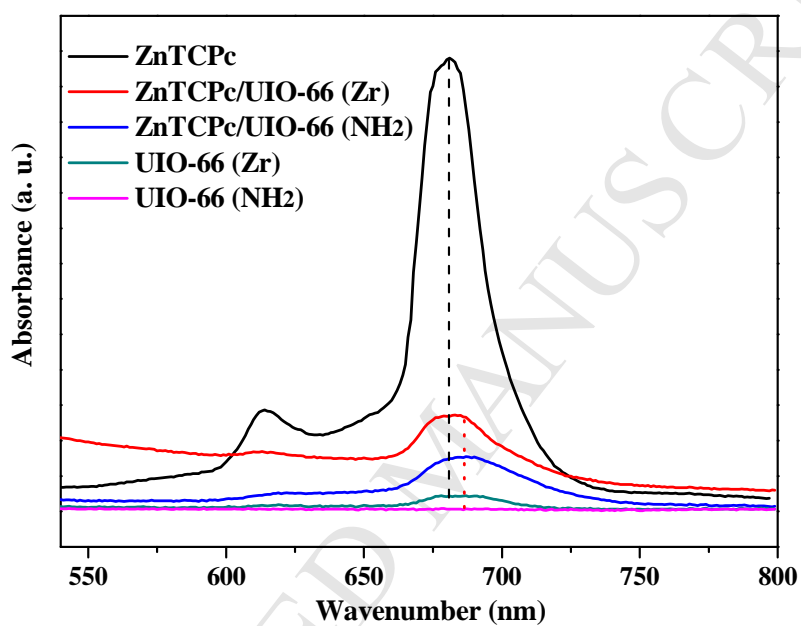


Fig. 7. UV-vis spectra of ZnTCPc, UIO-66 (Zr), UIO-66 (NH₂), ZnTCPc/UIO-66 (Zr) and ZnTCPc/UIO-66 (NH₂).

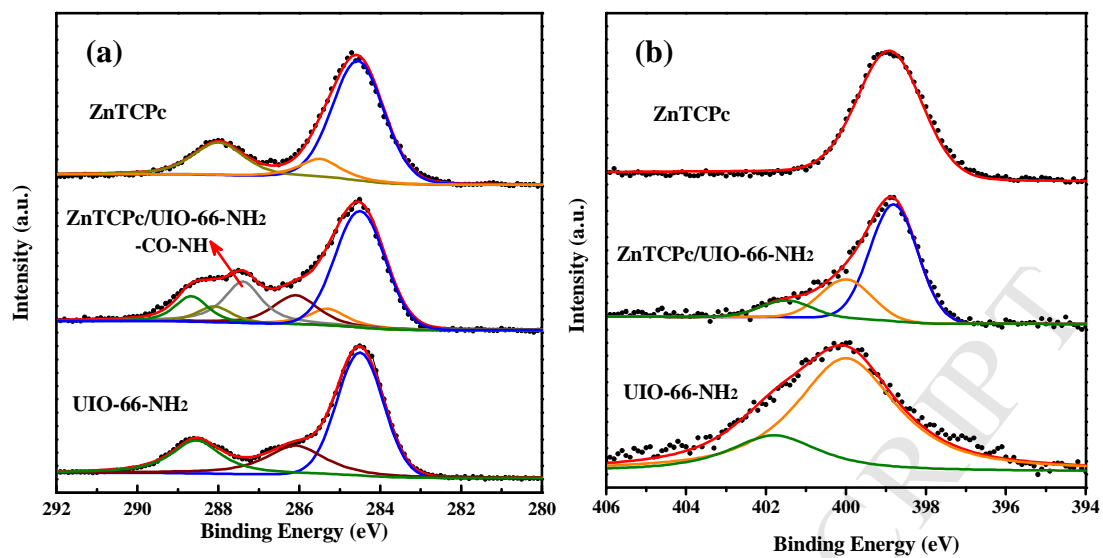


Fig. 8. High resolution XPS spectra of C 1s (a) and N 1s (b) obtained from ZnTCPC, ZnTCPC/UIO-66 (NH₂) and UIO-66 (NH₂).

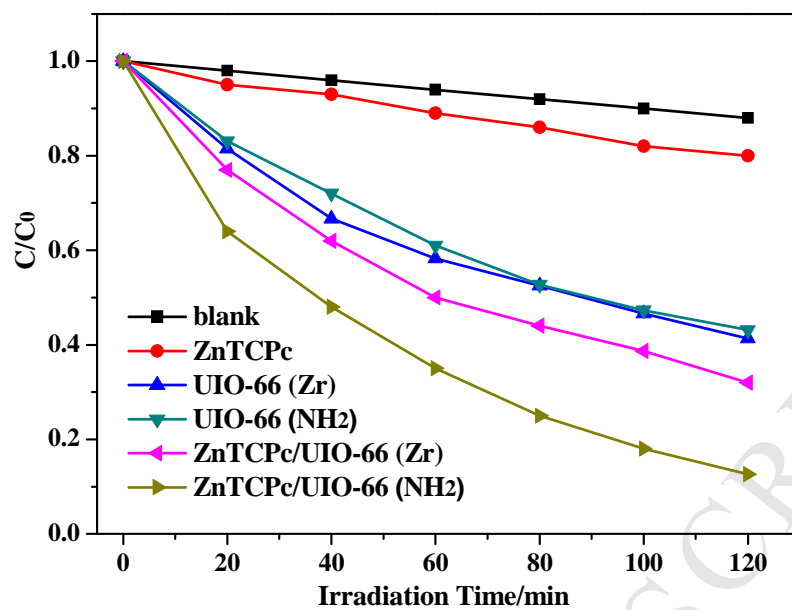


Fig. 9. Photocatalytic degradation of MB over the as-prepared samples under visible-light irradiation ($\lambda \geq 420$ nm).

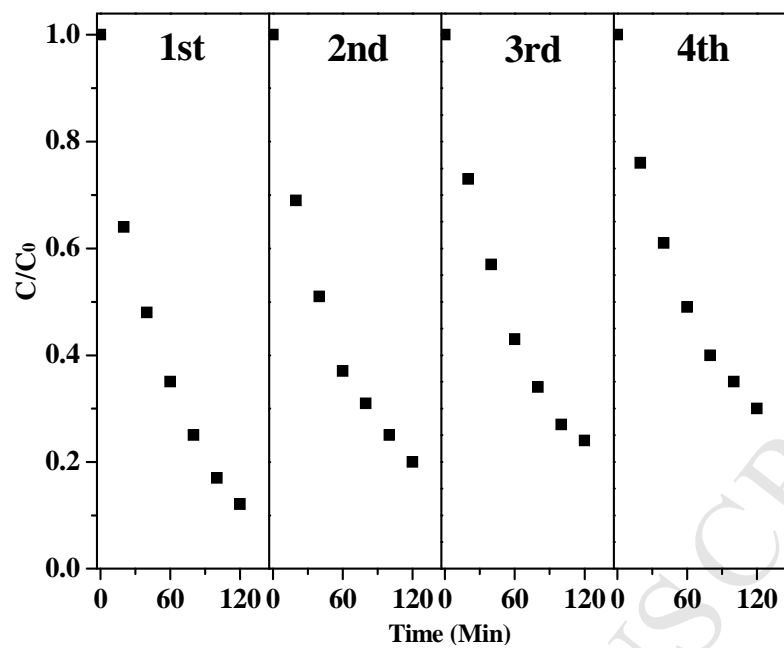


Fig. 10. Photocatalytic recycle degradation of MB over ZnTCPc/UIO-66 (NH₂) under visible-light irradiation ($\lambda \geq 420$ nm).

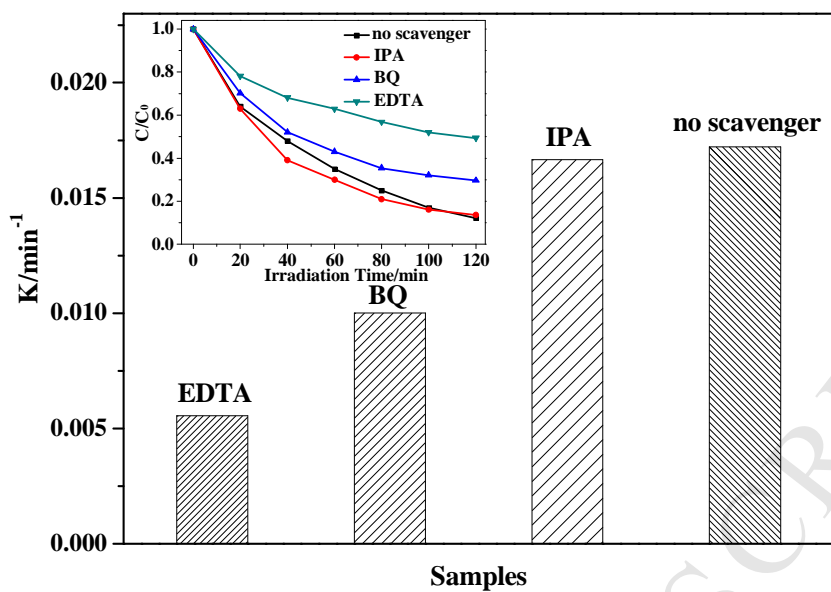


Fig. 11. Effects of different scavengers on the degradation of MB in the presence of ZnTCPc/UIO-66 (NH_2) under visible-light irradiation.

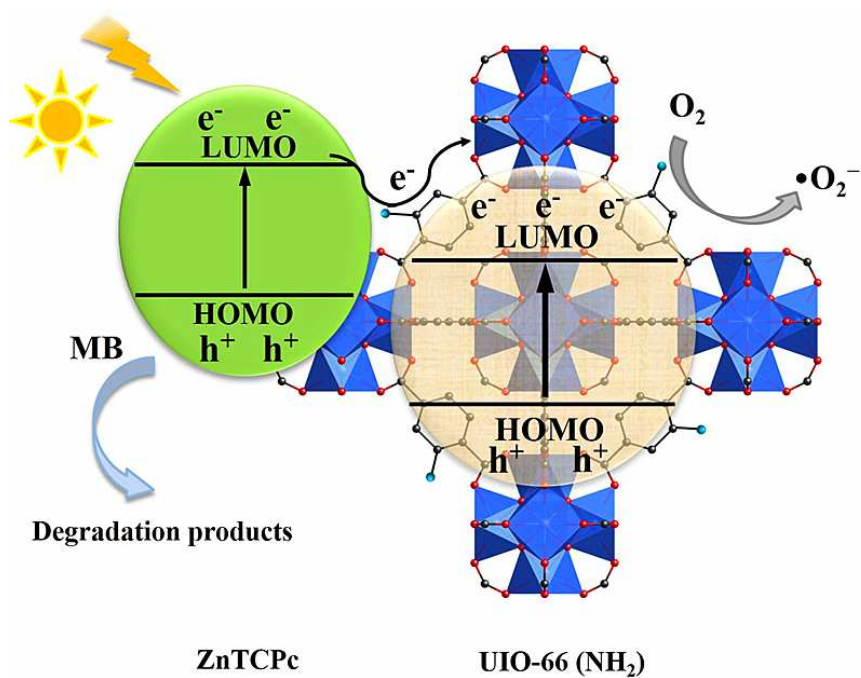


Fig. 12. Schematic of photocatalytic degradation of MB over the ZnTCPC/UIO-66 (NH₂) under visible light irradiation.

Highlights

- UIO-66 (NH₂) with ZnTCPc covalently was prepared via a facile condensation method.
- ZnTCPc/UIO-66 (NH₂) showed excellent visible-light-driven MB degrading activity.
- Tight interaction between ZnTCPc/UIO-66 (NH₂) led to highly catalytic stability.
- Photocatalytic activity was enhanced by high surface area and synergistic effect.